Journal of Catalysis 287 (2012) 102–113

Contents lists available at SciVerse ScienceDirect

Journal of Catalysis

journal homepage: www.elsevier.com/locate/jcat

On the promoting effect of Au on CO oxidation kinetics of Au–Pt bimetallic nanoparticles supported on SiO_2: An electronic effect?

Rachel P. Doherty [a,b,c,d], Jean-Marc Krafft [a,b], Christophe Méthivier [a,b], Sandra Casale [a,b], Hynd Remita [c,d], Catherine Louis [a,b], Cyril Thomas [a,b,*]

[a] UPMC, UMR 7197, Laboratoire de Réactivité de Surface, Case 178, 4 Place Jussieu, F-75005 Paris, France
[b] CNRS, UMR 7197, Laboratoire de Réactivité de Surface, 4 Place Jussieu, Case 178, F-75005 Paris, France
[c] Université de Paris-Sud, UMR 8000, Laboratoire de Chimie Physique, 15 rue Georges Clemenceau, F-91405 Orsay, France
[d] CNRS, UMR 8000, Laboratoire de Chimie Physique, 15 rue Georges Clemenceau, F-91405 Orsay, France

ARTICLE INFO

Article history:
Received 27 July 2011
Revised 19 October 2011
Accepted 11 December 2011
Available online 16 January 2012

Keywords:
Radiolysis
PtAu alloys
CO-FTIR
Restructuring of nanoparticles
CO oxidation kinetics
Turnover rates
Electron transfer

ABSTRACT

Bimetallic AuPt nanoparticles prepared by radiolysis with Au/Pt atomic ratios of 1.2 and 1.8 were deposited onto silica and calcined to remove the stabilizing polymers. During this sequence, they lose their core–shell structure and restructure as alloys. FTIR and XPS provide evidence for further AuPt NP restructuring under CO exposure and CO oxidation with Pt surface enrichment. A promoting effect of Au is found on the CO oxidation kinetics in the AuPt catalyst with the lower Au/Pt ratio. This effect is attributed to an electron enrichment of the Pt surface atoms due to charge transfer from Au to Pt, as indicated by XPS and CO-FTIR.

1. Introduction

Supported bimetallic nanoparticles have been shown to typically exhibit enhanced catalytic properties relative to their monometallic counterparts [1–8]. Recently, a significant amount of progress has been made in the preparation of supported bimetallic AuPt nanoparticles by dendrimer encapsulation [6,9,10] or from a single-source organometallic precursor such as $Pt_2Au_4(C{\equiv}C^tBu)_8$ [11,12], improving on traditional impregnation methods, which do not allow sufficient control over nanoparticle size, structure and composition. However, these preparation routes require the use of complex organic or organometallic molecules. Radiolysis has been shown to be a valuable tool in the preparation of bimetallic nanoparticles [13–15]. Here, simple polymers are employed as stabilizing agents allowing solution synthesis of bimetallic nanoparticles of controlled size and structure [15–18]. Radiolysis has also been shown to overcome the difficulty of preparing AuPt nanoparticles due to the Au/Pt miscibility gap from 18% to 98% Pt [19].

Silica was chosen as the support as it is relatively inert toward catalytic reactions [20] and does not exhibit strong metal-support interactions, in comparison to other available oxides such as TiO_2 [21], which has been shown to influence the catalytic properties of the metal nanoparticles [22].

The catalytic performance of SiO_2-supported AuPt nanoparticles has been previously studied [6,9,12,23,24]. Bimetallic AuPt nanoparticles have been reported to exhibit enhanced catalytic properties in comparison to their monometallic counterparts for instance for CO oxidation [6,9]. Explanations for the improvement in the catalytic behavior of supported AuPt nanoparticles include the presence of geometric [9] and electronic effects [7,11,12,25,26]. Reports to date of electronic effects on AuPt bimetallic nanoparticles have been contradictory. Some have reported possible electronic effects with electron transfer from Pt to Au [26] as in the direction expected by considering the difference in electronegativity of the two elements, while others have reported charge transfer in the opposite direction from Au to Pt [7,11,12,25]. For the Au-5d-transition metal alloying, calculations have revealed that charge transfer between the two metals does not follow their respective electronegativity [27].

In this article, for the first time, the kinetics of CO oxidation of SiO_2-supported AuPt nanoparticles is measured under stoichiometric conditions ($2CO/O_2 = 1$) to gain further insights into the

* Corresponding author. Address: Laboratoire de Réactivité de Surface, UPMC, UMR CNRS 7197, 4 place Jussieu, Case 178, F-75252 Paris Cedex 05, France. Fax: + 33 1 44 27 60 33.
E-mail address: cyril.thomas@upmc.fr (C. Thomas).

0021-9517/$ - see front matter © 2011 Elsevier Inc. All rights reserved.
doi:10.1016/j.jcat.2011.12.011

potential promoting effect of Au on the CO oxidation reaction catalyzed by Pt surface sites of bimetallic AuPt nanoparticles. The results are compared with those of SiO_2-supported Pt and Au, the full kinetics of the latter is also measured for the first time under these particular reaction conditions. Indeed, if CO oxidation kinetics of SiO_2-supported Pt nanoparticles has been documented [28], that of SiO_2-supported Au is to our knowledge not reported [29], probably due to the poor activity of Au/SiO_2 catalysts for this reaction. Recently, Chandler et al. reported CO oxidation kinetics in oxidizing mixtures ($0.1 < 2CO/O_2 < 0.3$) on AuNi or Au nanoparticles prepared by dendrimer encapsulation [30]. These authors did not determine the reaction order with respect to CO, which may, however, have provided valuable information.

2. Experimental

2.1. Catalyst preparation

The monometallic Pt/SiO_2 catalyst (1.96 wt.% Pt) was prepared by incipient wetness impregnation (IWI) of SiO_2 (Degussa Aerosil 380) with an aqueous solution of 0.04 mol L^{-1} $Pt(NH_3)_4(NO_3)_2$ (99.995%, Sigma–Aldrich), using a volume of solution of 2.5 ml g^{-1} of SiO_2. After aging at room temperature for 6 h, the catalyst was dried overnight at 120 °C. Au/SiO_2 (0.70 wt.% Au) was also prepared by IWI of SiO_2 with an aqueous solution of 0.02 mol L^{-1} $HAuCl_4$ ($HAuCl_4.3H_2O$, 99.99%, Sigma–Aldrich). After aging at room temperature for 6 h, the sample was washed with a 1 mol L^{-1} NH_3 aqueous solution adjusted to pH 8.5 with HCl according to the protocol outlined by Delannoy et al. [31] to remove the chloride ions and avoid the formation of large gold particles after thermal treatment. This was followed by washing with water several times, until a test by $AgNO_3$ no longer showed the presence of residual Cl^-, before drying at 60 °C for 48 h.

Bimetallic AuPt nanoparticles were prepared by radiolytic co-reduction [13,14] of a 50-ml aqueous solution of $HAuCl_4$ (5×10^{-4} mol L^{-1}) and H_2PtCl_6 (5×10^{-4} mol L^{-1}) (in the presence of the stabilizing polymers, polyacrylic acid (0.05 mol L^{-1} PAA, 2000 g mol^{-1}, Sigma–Aldrich) and polyvinyl alcohol (0.05 mol L^{-1} PVA, 85,000–124,000 g mol^{-1} Sigma–Aldrich) at a ratio of 1:1, for which nanoparticle deposition onto the SiO_2 support was found to be the most effective among the different ratios investigated. 2-propanol (0.1 mol L^{-1} Sigma–Aldrich) was added as a radical scavenger. Solutions were freshly prepared with a Au:Pt ratio of 1:1 in the absence of light to prevent possible photochemical reduction of Au and bubbled with N_2 prior to irradiation to remove oxygen. Radiolysis of the solution was carried out using a ^{60}Co panoramic gamma source [13] with a radiation dose rate of 2.2 kGy h^{-1}. Deposition of the radiolytically prepared nanoparticles was achieved by stirring SiO_2 into the nanoparticle solution for 24 h. The resulting $AuPt/SiO_2$ composites were washed repeatedly with water, to remove excess polymer, unwanted reaction by-products and until a $AgNO_3$ solution no longer tested positive for the presence of Cl^- ions. The resulting $AuPt/SiO_2$ samples were dried at 60 °C for 18 h before being finely ground.

Calcination of the $AuPt/SiO_2$ samples was performed at 400 °C for 2 h in O_2 (20%)/He (100 ml min^{-1}) in a quartz, fixed-bed, continuous-flow reactor.

2.2. Catalyst characterization

2.2.1. Chemical analysis

Chemical analysis of the supported catalysts was performed by inductively coupled plasma atom emission spectroscopy (ICP/AES) at the CNRS Centre of Chemical Analysis (Vernaison, France).

2.2.2. UV–vis spectroscopy

UV–visible spectra in liquid phase were obtained in a 2-mm quartz cell using a HP diode array HP8453 spectrophotometer.

2.2.3. Thermal gravimetric analysis (TGA-MS)

TGA experiments were performed using a SDT Q600 instrument (TA Instruments) coupled with a mass spectrometer (MS) (Thermostar GDS 301T3, Pfeiffer). Samples were heated at a rate of 3 °C min^{-1} under air (100 ml min^{-1}).

2.2.4. X-ray diffraction (XRD)

XRD patterns of the prepared samples were obtained on a SIEMENS D500 diffractometer with a Cu Kα monochromatized radiation (0.1548 nm) operated at 30 kV and 300 mA from 10° to 90° with a scanning rate of 0.013° s^{-1}.

2.2.5. H_2 and CO chemisorption

Platinum accessibility was evaluated via the irreversible chemisorption method using H_2 and CO as probe molecules. These measurements were performed in a static mode at 25 °C using a conventional volumetric apparatus (Belsorp max, Bel Japan). Typically, 0.14 g of catalyst was used. Before the H_2 or CO chemisorption measurements, the catalyst was first reduced in H_2 (50 mL/min) at 500 °C for 2 h (3 °C/min heating rate) with subsequent evacuation at 400 °C for an additional 2 h. Then, the sample was cooled down under vacuum to 25 °C. Two H_2 or CO adsorption isotherms were obtained. After the first isotherm, the catalyst was evacuated again for 2 h at 25 °C. The amounts of total and reversible H_2 or CO uptakes were then estimated by extrapolating the quasi-linear portions of the isotherm to zero pressure. The difference between these two values gave the amount of irreversible H_2 or CO uptake, from which the number of accessible Pt atoms was calculated assuming stoichiometries of 1 hydrogen atom or 1 CO molecule per surface Pt atom.

2.2.6. Transmission electron microscopy (TEM)

TEM analysis of the metal particles was performed using a JEOL 100 CX II microscope. The size limit for Pt and Au particles detection is in principle about 1 nm. Particle size measurements were performed particle by particle, using ITEM software on digitized micrographs. The average metal particle sizes, d, were determined from the measurement of at least 130 metal particles, and d was calculated using the following formula: $d = \Sigma n_i d_i / \Sigma n_i$, where n_i is the number of particles of diameter d_i. High-resolution TEM and EDX were performed using a JEOL 2010 microscope.

2.2.7. X-ray photoelectron spectroscopy (XPS)

XPS spectra were collected on a SPECS (Phoibos MCD 100) X-ray photoelectron spectrometer, using a Al Kα ($h\nu$ = 1486.6 eV) monochromated radiation source having a 400 W electron beam power and a 0.5 × 2 mm spot size. The emission of photoelectrons from the sample was analyzed at a takeoff angle of 90° under ultra high vacuum conditions (1×10^{-8} Pa). XP spectra were collected at pass energy of 10 eV for C_{1s}, Si_{2p}, Pt_{4f} and Au_{4f} core XPS levels. Charge compensation was applied during acquisition with the use of a flood gun (4 eV, 300 μA emission current). Spectrum processing was carried out using the Casa XPS software package and Origin 7.1 (Origin Lab Corporation). All materials were analyzed after being stored in air under ambient conditions following their pretreatment. For Pt/SiO_2 and $AuPt(1.2)/SiO_2$ initially reduced at 500 °C under H_2, XPS analysis was also carried out after the catalysts were reduced in the pretreatment chamber of the XPS facility at 200 and 400 °C, respectively, for 10 min in flowing H_2(10%)/Ar, thus avoiding sample exposure to the ambient atmosphere. These particular samples will be denoted as "reduced

XPS" to be distinguished from the same catalysts reduced in H_2 and exposed to ambient air (denoted as "reduced").

2.2.8. Fourier transform infrared spectroscopy of adsorbed CO (CO-FTIR)

CO-FTIR spectra of adsorbed CO on the SiO_2-supported samples were collected in transmission on a Bruker Vector 22 FTIR spectrometer equipped with a liquid N_2-cooled MCT detector and a data acquisition station. A total of 128 scans were averaged with a spectral resolution of 2 cm^{-1}. The samples were pressed into self-supporting wafers of about 8–12 mg cm^{-2} (16–25 mg for wafers of 16 mm diameter). The wafers were loaded in a moveable glass sample holder, equipped on top with an iron magnet, and inserted in a conventional Pyrex-glass cell (CaF_2 windows) connected to a vacuum system. The iron magnet allowed for the transfer of the catalyst sample from the oven-heated region to the infrared light beam. Before CO adsorption, the catalysts were submitted to a dynamic (50 cm^3 min^{-1}) reducing pretreatment (5% H_2 in Ar, Air Liquide, 99.999%) at 500 °C for 2 h at atmospheric pressure. The samples were then evacuated (7.5×10^{-7} Torr) at 500 °C for 30 min. Finally, the temperature was decreased to RT under dynamic vacuum. The samples were then exposed to CO (Air Liquide, 99.999%) additionally purified by passing through a liquid nitrogen trap. The spectrum at RT of the pretreated sample was used as a reference and subtracted from the spectra of the sample exposed to CO.

2.3. Catalytic experiments

2.3.1. Benzene hydrogenation

Before benzene hydrogenation, the catalyst sample (0.050 g deposited on a plug of quartz wool inserted inside a quartz reactor) was heated in flowing H_2 (100 cm^3 NTP min^{-1}) at atmospheric pressure with a heating rate of 3 °C min^{-1} up to 500 °C and held at this temperature for 2 h. After cooling to 50 or 115 °C under H_2, the reaction was started. The partial pressure of benzene (C_6D_6, Aldrich) was 51.8 Torr (1 Torr = 133 Pa), and the total flow rate was 107 cm^3 NTP min^{-1} with H_2 as balance. The composition of the effluent was analyzed using an online gas chromatograph (Hewlett Packard 5890, FID) equipped with a PONA (paraffins–olefins–naphthenes–aromatics; HP, 50 m long, 0.20 mm i.d., 0.5 μm film thickness) capillary column. Cyclohexane was the only product detected.

2.3.2. CO oxidation kinetics

Before runs, the catalyst samples (about 15 mg for Au/SiO_2, $AuPt(1.2)/SiO_2$ and $AuPt(1.8)/SiO_2$, and 10 mg of a mechanical mixture of 10 wt% of Pt/SiO_2 in SiO_2) were submitted to a temperature-programmed reduction from RT to 500 °C (3 °C min^{-1}) under H_2 (Air Liquide, 100 cm^3 NTP min^{-1}) and held at this temperature for 2 h. The catalyst temperature was then decreased to 280 °C under H_2. The kinetic study was conducted in a U-type quartz dynamic differential microreactor (12 mm i.d.) with a total flow rate of 50 mL min^{-1}. The synthetic gas mixture was fed from independent mass flow controllers (Brooks 5850). The reactor outflow was analyzed using a μ-GC (Varian, CP4900) equipped with two channels. The first channel used a 5A molecular sieve column (80 °C, 150 kPa He, 200 ms injection time, 30 s backflush time) and was used to quantify O_2 and CO. The second channel was equipped with a poraplot Q column (100 °C, 150 kPa He, 50 ms injection time, 6 s backflush time) and was used to quantify CO_2. CO conversions were calculated as follows: X CO (%) = $[CO_2]/[CO]_i \times 100$, where $[CO_2]$ and $[CO]_i$ were the concentration of CO_2 measured at the outlet of the reactor and the initial concentration of CO, respectively.

The kinetic parameters reported in the present work were obtained at steady-state, while the reactor was operated isothermally and as close to a differential reactor as possible by limiting the conversion to <10%. The CO reaction order was determined at 280 °C under reactive gas mixtures by maintaining the O_2 concentration at 0.5% and varying the CO concentration from 0.5% to 1.5%. The O_2 reaction order was determined at the same temperature by maintaining the CO concentration at 1.0% and varying the O_2 concentration from 0.3% to 0.7%. The apparent activation energy was determined under stoichiometric conditions (1.0% CO and 0.5% O_2 in He) at reaction temperatures of 270–300 °C.

3. Results and discussion

3.1. Catalyst characterization

Details of the prepared catalysts are summarized in Table 1. Prior to analysis, the samples were either calcined in the case of the bimetallics or reduced in the case of the monometallics. The metal weight loadings of the monometallic references were 1.96 and 0.70 wt.% for Pt/SiO_2 and Au/SiO_2, respectively. The resulting supported bimetallic catalysts were 0.45 wt.% Au and 0.25 wt.% Pt on SiO_2 (Au/Pt = 1.8) and 0.45 wt.% Au and 0.36 wt.% Pt on SiO_2 (Au/Pt = 1.2). From here on, these will be referred to as $AuPt(1.8)/SiO_2$ and $AuPt(1.2)/SiO_2$, respectively. Overall, the amount of Pt in the bimetallic catalysts was always lower than the amount of Au.

3.1.1. UV–vis of the AuPt colloids formed by radiolysis

UV–vis absorption spectra of the PAA/PVA stabilized AuPt nanoparticles in solution prior to deposition onto SiO_2 are displayed in Fig. 1. A plasmon band at 540 nm is visible in the UV–vis spectrum of the colloids corresponding to the higher Au/Pt ratio (1.8). This plasmon resonance, which is well documented as being due to the plasmonic resonance of nanosized Au particles [32,33], is almost, if not completely, non-existent in the spectrum of the nanoparticles with the lower Au/Pt ratio (1.2). The growth of bimetallic AuPt nanoparticles by this method has previously been reported by Remita and coworkers [14] who concluded that the nanoparticles formed under similar conditions to ours were of a Au_{core}-Pt_{shell} structure. Indeed, previous experiments have shown that radiolysis of a solution containing $PtCl_4^{2-}$ and $AuCl_4^-$ leads to formation of Au_{core}–Pt_{shell} NPs of typical diameter 3–4 nm at low dose rate (by γ-irradiation), or to alloyed Au–Pt nanoparticles of typical diameter 2–3 nm at high dose rate (electron beam irradiation) [13,34]. This difference in the NP structure is due to electron transfer from Pt complexes or nascent Pt^0 induced by radiolysis to gold complexes (Au^{III} or Au^{I}) occurring only at low dose rate when the reduction kinetics is slow. At high dose rate by electron beam irradiations, the reduction of all ions can be achieved rapidly before any intermetallic electron transfer can occur, leading to alloyed nanoparticles. In the case of a perfect Au_{core}–Pt_{shell} structure, no gold plasmon is expected, and this is indeed, very nearly, the case for the AuPt colloids with Au/Pt = 1.2. Though it cannot be definitively ascertained from this almost complete absence whether the nanoparticles are core–shells or alloys, it strongly suggests that the Au–Pt (1.2) sample is bimetallic. It is however appreciated that the bimetallic nature of the nanoparticles can only be implied and not fully determined by UV–vis spectra alone. Further results will go onto strengthen and confirm this bimetallic interpretation of the results. The plasmon resonance of the colloids of AuPt(1.8), more Au-rich, is weak and implies that these nanoparticles are either bimetallic with the presence of Pt in the particles diminishing the intensity of the Au resonance at 540 nm, or that there is a small percent of monometallic Au nanoparticles in an otherwise

Table 1
Summary of the supported catalysts prepared by IWI (monometallic) or radiolytic γ reduction followed by deposition onto the SiO_2 support (bimetallic). Metal particle diameters determined by TEM are also shown at different catalyst preparation stages.

Catalyst	Preparation method	Au loading (wt.%)	Pt loading (wt.%)	Preparation stage	TEM size (nm)	Number of sized nanoparticles
Pt/SiO_2	Impregnation		1.96	H_2/500 °C	1.9	518
AuPt(1.2)/SiO_2	γ-irradiation	0.45	0.36	Solution (before deposition onto SiO_2)	3.5	257
				Deposited onto SiO_2 and dried at 60 °C	3.7	131
				Calcined at 400 °C/2 h	4.2	219
				H_2/500 °C followed by CO/O_2 reaction	4.6	165
AuPt(1.8)/SiO_2	γ-irradiation	0.45	0.25	Solution (before deposition onto SiO_2)	3.5	320
				Deposited onto SiO_2 and dried at 60 °C	3.4	273
				Calcined at 400 °C/2 h	4.4	242
				H_2/500 °C followed by CO/O_2 reaction	4.6	455
Au/SiO_2	Impregnation	0.70		H_2/500 °C	3.7	391

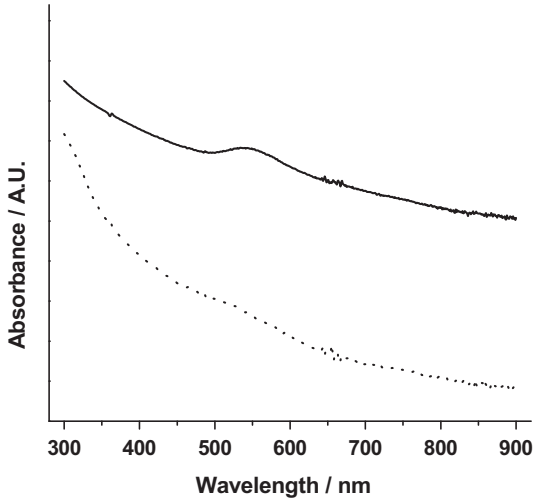

Fig. 1. UV–visible spectra of the AuPt colloids in water (... AuPt(1.2), — AuPt(1.8)).

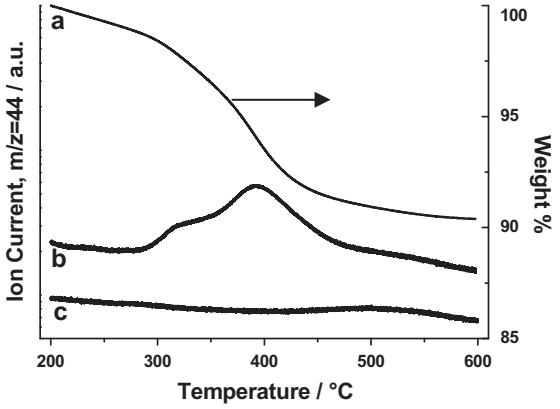

Fig. 2. TGA results on AuPt (1.8)/SiO_2, (a) weight change (sample with no prior heat treatment), (b) CO_2 trace associated with weight change (a), (c) CO_2 trace after calcination at 400 °C for 2 h.

bimetallic sample. XRD and TEM results will show later that the last hypothesis is more probable.

3.1.2. Decomposition of stabilizing polymers followed by TGA

Before the catalytic properties of the bimetallic nanoparticles supported on silica can be investigated, it is necessary to remove the stabilizing polymers. In order to optimize the calcination temperature and minimize potential nanoparticle sintering, TGA-MS was used to investigate polymer decomposition as a function of temperature, thus allowing the organic molecules to be decomposed at the lowest temperature possible. TGA-MS of AuPt(1.8)/SiO_2 (Fig. 2, trace b) shows a maximum in the release of CO_2 at 400 °C which correlates with the most significant decrease in the weight of the sample (Fig. 2, trace a). TGA-MS was repeated after calcination at 400 °C (AuPt(1.8)/SiO_2, 400 °C/2 h), verifying that the polymers had been successfully removed (Fig. 2, trace c), no decrease in weight was observed for this sample. Similar results (not shown) were also found for AuPt(1.2)/SiO_2.

3.1.3. XRD

XRD patterns of the samples are shown in Fig. 3. The diffraction patterns of reduced Pt/SiO_2 (a) and Au/SiO_2 (b) show diffraction peaks consistent with those of Pt and Au nanoparticles, respectively. The broad intense contribution at 23 ° is consistent with the presence of amorphous SiO_2. XRD patterns of the two SiO_2-supported bimetallic nanoparticles before and after calcination and after CO oxidation are shown in Fig. 3c and d. The similarity in the lattice parameters of Au and Pt along with the broadness of the peaks makes resolving the pattern of AuPt(1.2)/SiO_2 difficult. The pattern of AuPt(1.8)/SiO_2 can be seen to contain additional sharper peaks in the appropriate position for Au. These peaks are believed to be due to the presence of a small number of larger Au-only particles (8–12 nm). These larger particles, as hinted on in the UV–visible section, will be later seen in the electron microscopy section and accounted for just 1% of the total number of particles.

The Scherrer equation was used to calculate the average diameter of the Au (4.4 nm) and Pt (22 nm) nanoparticles in the SiO_2-supported samples after reduction and the AuPt nanoparticles in the AuPt(1.2)/SiO_2 sample before (3.7 nm) and after (3.9 nm) calcination (The Scherrer equation was only performed on the samples exhibiting peaks with a symmetrical distribution of intensity). Utilization of the Scherrer equation to calculate nanoparticle diameters for AuPt(1.8)/SiO_2 was hindered by the presence of the sharp peak due to a small percentage of larger Au nanoparticles. On Pt/SiO_2, the size of the Pt nanoparticles obtained by this method (22 nm) is considerably larger than expected, and it is suspected that the XRD pattern in this case has been distorted and overpowered by the presence of a small percentage of large Pt nanoparticles, this was later confirmed by H_2 and CO chemisorption measurements (Section 3.1.4.) and electron microscopy (Section 3.1.5.).

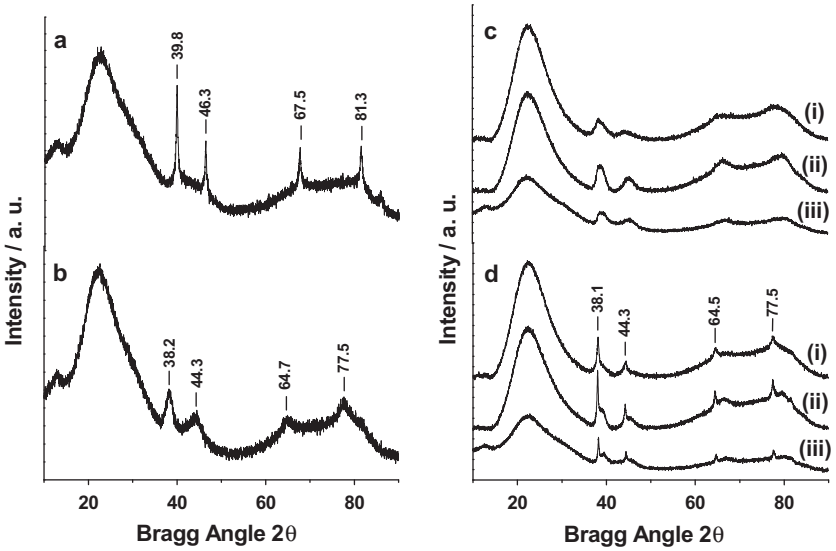

Fig. 3. XRD patterns of SiO_2-supported catalysts, (a) Pt/SiO_2 reduced, (b) Au/SiO_2 reduced, (c) $AuPt(1.2)/SiO_2$, and (d) $AuPt(1.8)/SiO_2$, (i) before calcination, (ii) after calcination, (iii) after reduction and CO/O_2 reaction. The peak labels denote the associated 2θ values in degrees.

3.1.4. H_2 and CO chemisorption

H_2 and CO chemisorption data (not shown) lead to a Pt dispersion of 30.9% and 32.5%, respectively, rounded to 31.7 ± 0.8% for the Pt/SiO_2 catalyst, to which corresponds a mean particle size of the Pt particles of about 3.5 nm [35].

The first and second isotherms of H_2 or CO overlap on $AuPt(1.2)/SiO_2$ (not shown). This prevents the use of H_2 and CO chemisorption as a tool to estimate the number of Pt atoms on the surface of the bimetallic particles and indicates that the number of Pt surface atoms is extremely low on the bimetallic particles, in agreement with the CO-FTIR and benzene hydrogenation results which will be shown later (Sections 3.1.7 and 3.2.1).

3.1.5. TEM

TEM images were taken of Pt/SiO_2 and Au/SiO_2 after reduction, and of $AuPt(1.2)/SiO_2$ and $AuPt(1.8)/SiO_2$ after different catalyst preparation stages. The average nanoparticle sizes are listed in Table 1. Supported Pt and Au monometallic nanoparticles were found to be on average 1.9 nm and 3.7 nm in diameter, respectively. The size of the Au/SiO_2 nanoparticles is in reasonable agreement with that obtained by the Scherrer equation (4.4 nm). However, as suspected, TEM images showed that the Pt/SiO_2 sample contained a small percentage of large (>20 nm) Pt nanoparticles. These accounted for less than 1% of the nanoparticles and are responsible for the lack of coherence between the Scherrer (22 nm) and TEM (1.9 nm) size estimations. The fact that the mean Pt particle size estimated to be 3.5 nm from the chemisorption data (Section 3.1.4) is about twice as big as that estimated from TEM is attributed to the presence of the large particles, as detected by XRD (Section 3.1.3). For the calculation of the benzene hydrogenation and CO oxidation turnover rates, which will be shown later (Section 3.2), the Pt dispersion estimated from the chemisorption data (31.7%) was thus considered.

The two bimetallic $AuPt/SiO_2$ samples follow the same trend. The initial nanoparticles deposited onto the TEM grid from solution immediately after radiolysis, are, for both $AuPt/SiO_2$ samples, 3.5 nm in diameter on average. After deposition onto the SiO_2, there is a small but not significant change ($\leqslant$0.2 nm) in the average size of both samples, potentially due to the poorer contrast between SiO_2 and the nanoparticles, making visualization of the nanoparticles, particularly those with the smallest diameters, more difficult. After calcination (400 °C/2 h/air), an increase in diameter to 4.2–4.4 nm can be seen for both $AuPt(1.2)/SiO_2$ and $AuPt(1.8)/SiO_2$. The diameters of the AuPt nanoparticles in the $AuPt(1.2)/SiO_2$ catalyst before (3.7 nm) and after calcination (4.2 nm) are in good agreement with those obtained by Scherrer analysis of the XRD data, 3.7 nm and 3.9 nm, respectively. A similar smaller further increase to 4.6 nm is observed after the $AuPt(1.2)/SiO_2$ and $AuPt(1.8)/SiO_2$ catalysts were reduced (500 °C/2 h/H_2) and exposed to CO/O_2 at up to 300 °C for 30 h. Calcination and reduction steps therefore result in a small degree of sintering of the supported nanoparticles.

The nanoparticle size distribution in the AuPt samples at each stage is reasonably narrow in solution and after deposition on silica, but is broadened to a small degree after calcination (Fig. 4). H_2 reduction followed by CO/O_2 is shown to have no significant effect on the size distribution.

A representative HRTEM image of $AuPt(1.8)/SiO_2$ after CO oxidation is shown in Fig. 5a. The *d*-spacings between adjacent lattice fringes of the $AuPt(1.8)/SiO_2$ catalyst after exposure to CO/O_2 were measured for several nanoparticles and found to be 2.30 Å. This value lies between bulk fcc-Au (1 1 1) at 2.355 Å and bulk fcc-Pt (1 1 1) at 2.265 Å, which is a good indication of alloy structuring. Assuming there to be a linear trend between composition and lattice spacing, which has been reported for AuPt nanoparticles [36,37], one can calculate that the Au/Pt atomic ratio is equal to 1.6, which is close to the ratio given by chemical analysis.

EDX analysis was performed on the isolated AuPt nanoparticle of the $AuPt(1.8)/SiO_2$ sample shown in Fig. 5a, using a beam spot size of 10–15 nm. The presence of both Au and Pt in the same nanoparticle can clearly be seen on the EDX spectrum (Fig. 5b), confirming its bimetallic nature. The measurement was performed on five other isolated nanoparticles ranging in size from 5.1 to 7.8 nm within the $AuPt(1.8)/SiO_2$ sample, all showing the presence of both Au and Pt with an almost constant Au/Pt intensity ratio of between 1.0 and 1.3 (these values are not quantitative as no calibration was made). Because of the lack of any contrast between the two elements Au and Pt, the HRTEM images cannot provide any information on the particle structure.

3.1.6. XPS

XPS was used to investigate changes in the electron density of Pt and in the nanoparticle composition at different catalyst preparation stages of the $AuPt(1.2)/SiO_2$ sample. The spectra showing the

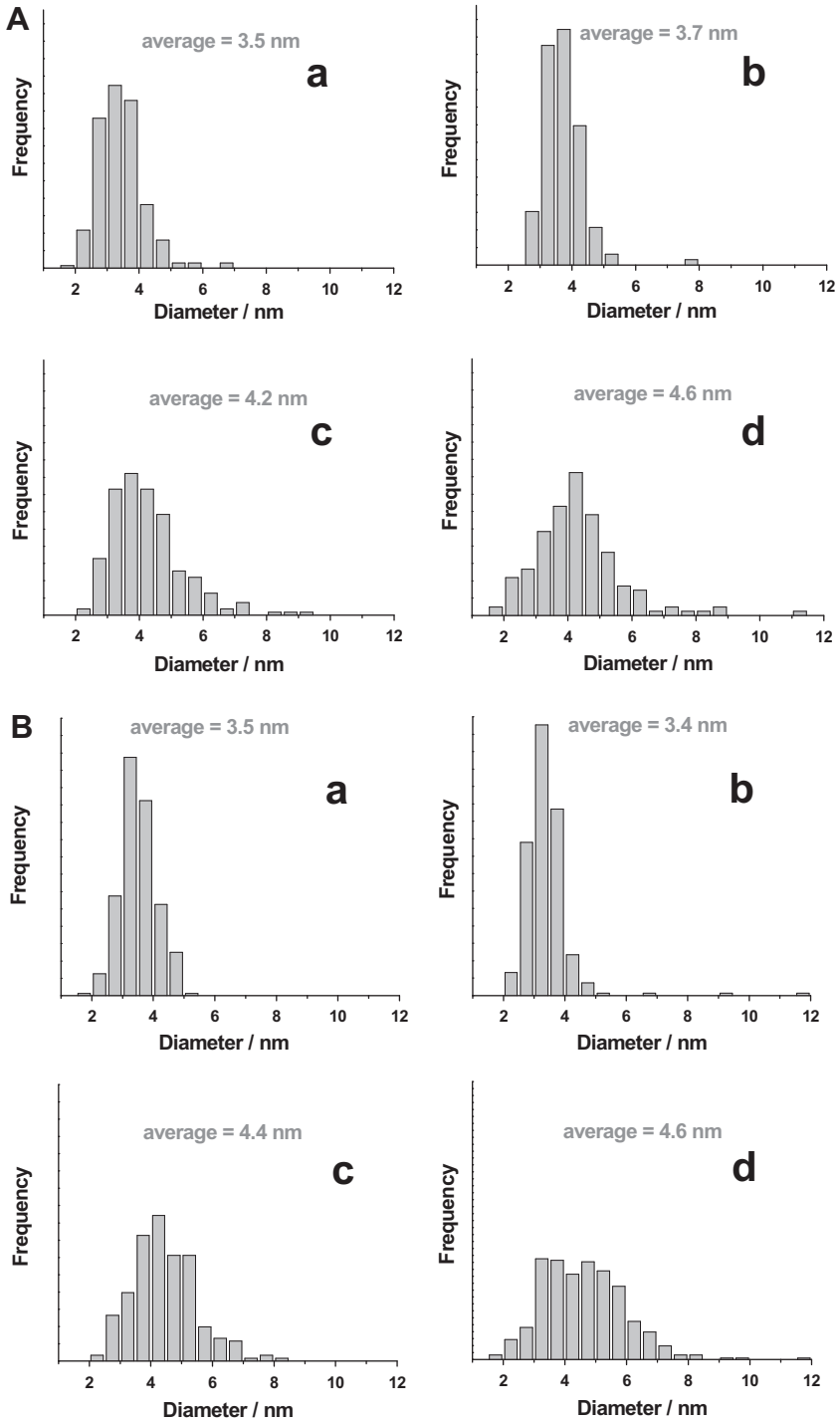

Fig. 4. Size distributions of AuPt nanoparticles; (A) AuPt(1.2)/SiO_2, and (B) AuPt (1.8)/SiO_2 at different catalyst preparation stages, (a) in solution, (b) after deposition onto SiO_2 and drying at 60 °C, (c) after calcination at 400 °C, (d) after reduction at 500 °C followed by reaction CO/O_2.

Au $4f_{7/2}$ and Pt $4f_{7/2}$ core-level peaks of Pt/SiO_2, AuPt(1.2)/SiO_2 and Au/SiO_2 are displayed in Fig. 6. The corresponding XPS data (BE, FWMH and atomic compositions) are listed in Table 2. The spectra (Fig. 6) clearly show the presence of metallic Au and/or Pt in the nanoparticles, whose binding energies agree with those reported previously [38,39], i.e. about 84 and 71 eV for Au $4f_{7/2}$ and Pt $4f_{7/2}$ core-levels (Table 2). As also reported recently for AuPt particles [40], it can be seen that the Pt $4f_{7/2}$ binding energy is lower for AuPt(1.2)/SiO_2 than for Pt/SiO_2, whereas that of Au $4f_{7/2}$ for AuPt(1.2)/SiO_2 remains similar to that found for Au/SiO_2 (Table 2). The FWHM of the Au $4f_{7/2}$ and Pt $4f_{7/2}$ peaks is about 2.3 and 3.0 eV (Table 2), respectively. The FWHM of the Au $4f_{7/2}$ peaks is much smaller than that reported by Radnik et al. on Au/SiO_2 [41]. In contrast, the FWHM of the Pt $4f_{7/2}$ peaks is greater than that expected from literature data [42] even for the samples that were reduced in H_2 at 500 °C (Table 2, reduced). This may be attributed to the presence of oxidized Pt species, due to Pt reoxidation upon exposure to air prior to transferring in the XPS facility, which would lead to a broadening of the Pt $4f_{7/2}$ peaks. To ascertain such an assumption, the Pt/SiO_2 and AuPt(1.2)/SiO_2 reduced samples were further

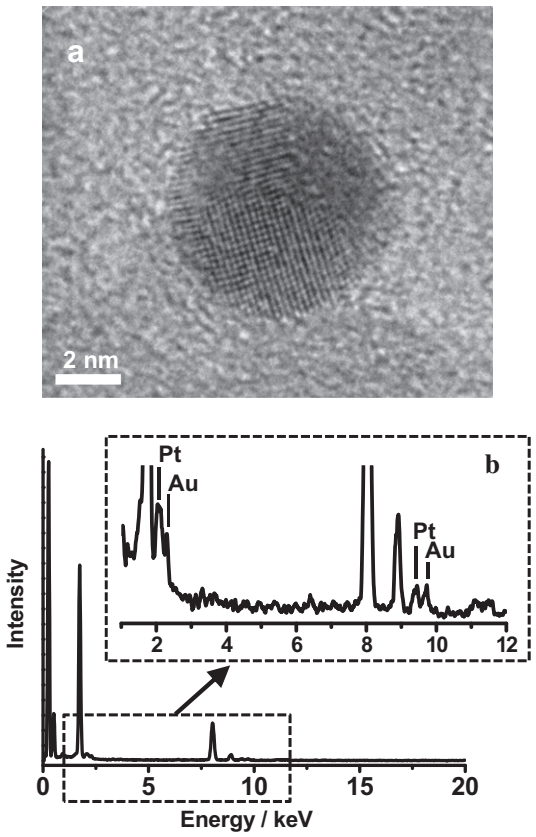

Fig. 5. (a) HRTEM of one metal particle of AuPt (1.8)/SiO_2 after reduction and CO/O_2 reaction, (b) EDX spectrum of the nanoparticle in image (a).

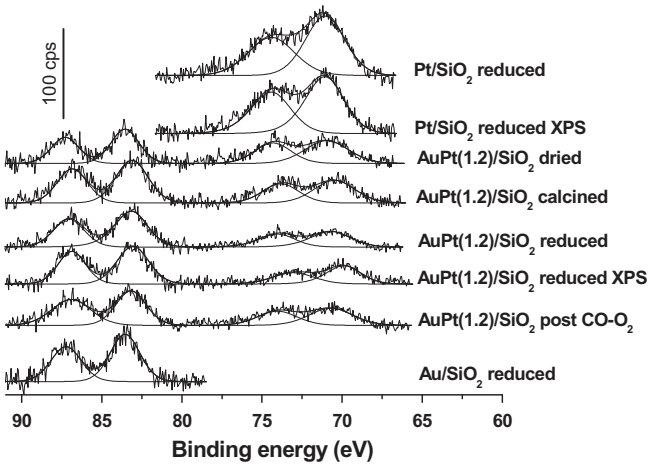

Fig. 6. XP Spectra and the corresponding decomposition of Au_{4f} and Pt_{4f} peaks of Pt/SiO_2, AuPt(1.2)/SiO_2 and Au/SiO_2 after different pretreatments.

reduced in H_2(10%)/Ar in the pretreatment chamber of the XPS facility for 10 min at 200 and 400 °C, respectively, thus avoiding exposure to air before XPS analysis (samples denoted as reduced XPS in Table 2). In this particular case, the FWHM of the Pt $4f_{7/2}$ peaks of Pt/SiO_2 and AuPt(1.2)/SiO_2 decreases from 2.9 to 2.6 and 2.4 eV, respectively. These FWHM values agree better with those reported earlier for metallic Pt [42], confirming that the broadening of the Pt $4f_{7/2}$ peaks is likely attributable to the presence of oxidized Pt species due to exposure to air. It is also noteworthy that the FWHM of the Au $4f_{7/2}$ peak of the AuPt(1.2)/SiO_2 further reduced in the pretreatment chamber of the XPS facility remains unchanged. This, together with the relatively narrow FWHM (~2.3 eV), demonstrates that Au is present only as metallic Au in the samples investigated in the present work, regardless of the pretreatments applied. More interesting from the XPS results summarized in Table 2, the Pt $4f_{7/2}$ binding energy of AuPt(1.2)/SiO_2 decreases to a significant extent when further reduced in the pretreatment chamber of the XPS facility (70.0 eV, Table 2). It must also be emphasized that this binding energy is about 1 eV lower than that expected for metallic Pt attesting to an electron transfer from Au to Pt in the bimetallic particles, in agreement with the CO-FTIR results which will be shown later (Section 3.1.7).

Table 2 also shows that the Au/Pt ratio of the supported nanoparticles is changed significantly by the environmental conditions to which they were exposed. The Au/Pt ratio of the dried AuPt(1.2)/SiO_2 sample is lower than that given by chemical analysis (Table 1, Au/Pt ~ 1.2). This is consistent with the reduction of the Pt species onto gold seeds and the formation of Pt_{core}–Au_{shell} colloids in the course of the radiolysis process [14]. After oxidizing and reductive pretreatments, the Au/Pt ratio becomes much larger than that calculated from the metal composition determined by chemical analysis, attesting to a surface gold enrichment in line with predictions from thermodynamic data [26,43]. This shows that the nanoparticles are not homogeneous alloys and that Au has a preference over Pt to reside in the outer shell of the nanoparticles. These results also attested that particle restructuring had occurred during calcination and reduction steps. Finally, the Au/Pt ratio of the bimetallic nanoparticles decreases to the value expected for the composition of the homogeneous alloy after CO–O_2 reaction, indicating that CO favors the migration of Pt toward the surface of the nanoparticles, as also already noticed earlier for Pd in AuPd [44–47] and Pt in PtCu [47] alloys. Changes in the structure of the AuPt nanoparticles under CO atmospheres have been further investigated by CO-FTIR.

3.1.7. CO-FTIR

Infrared spectroscopy of adsorbed CO was performed on Pt/SiO_2, Au/SiO_2, AuPt(1.2)/SiO_2 and AuPt(1.8)/SiO_2 reduced *in situ* (500 °C/2 h/5% H_2 in Ar) prior to measurement. The results are displayed in Figs. 7 and 8. Fig. 7a (under 1.1 Torr of CO: black curve) shows the FTIR-CO absorption spectrum of Pt/SiO_2, which contains absorption bands at 2084 cm^{-1} and 1849 cm^{-1}. These bands are attributed to the vibration of CO linearly (noted Pt–CO) and bridged bound to Pt, respectively, according to literature [48–50]. After evacuation of gas-phase CO (Fig. 7a, gray curve), the Pt–CO band shifts to lower wavenumbers at 2081 cm^{-1}. This is attributed to a decrease in the coverage and the dipole–dipole coupling of the Pt–CO species [50]. The FTIR-CO spectrum of Au/SiO_2 displayed in Fig. 7b contains a single band at 2116 cm^{-1} due to linearly adsorbed CO on reduced gold sites [44,51–56] (noted Au–CO). As in the case of former studies, no bridge-bound Au_n–CO species were observed [44,57,58].

Initially, after exposure of AuPt(1.2)/SiO_2 to an atmosphere of CO (1.1 Torr, RT), a strong band assigned to Au–CO is observed at 2111 cm^{-1} (Fig. 8a, spectrum (i)), which is in close agreement with the Au–CO band observed for the monometallic Au/SiO_2 catalyst (2116 cm^{-1}, Fig. 7b). Two smaller and broader bands centered around 2042 and 1870 cm^{-1}, and assigned to linear and bridged Pt–CO species, are also observed. The band at 2042 cm^{-1} is, however, significantly broader and shifted by 39 cm^{-1} from that observed for the monometallic Pt/SiO_2 (2081 cm^{-1}, Fig. 7a). After acquisition of spectrum (i) in Fig. 8a, the CO atmosphere was evacuated (10^{-6} mbar, RT), upon which a quasi-instantaneous disappearance of the Au–CO peak, spectrum (i) in Fig. 8b, was observed. The ease with which CO could be desorbed from Au sites confirms that CO is weakly adsorbed to Au sites [9,12]. This disappearance of the Au–CO band also coincides with an increase in intensity, and a change in shape of the linear Pt–CO band, which

Table 2
XPS data for each catalyst after different pretreatments.

Catalyst	Pretreatment	Pt $4f_{7/2}$ (FWHM) (eV)	Au $4f_{7/2}$ (FWHM) (eV)	Pt (at.%)	Au (at.%)	Si (at.%)	C (at.%)	Au/Pt ratio	Au/Si ratio ($\times 10^{-3}$)
Pt/SiO_2	Reduced	71.1 (2.9)	–	0.055	–	36.1	1.3	–	–
	Reduced XPS[a]	71.1 (2.6)	–	0.047	–	33.6	1.3	–	–
$AuPt(1.2)/SiO_2$	Dried	71.0 (3.1)	83.5 (2.2)	0.022	0.019	30.9	13.9	0.9	0.62
	Calcined	70.5 (3.0)	83.1 (2.4)	0.017	0.023	31.3	1.8	1.4	0.73
	Reduced	70.7 (2.9)	83.2 (2.3)	0.015	0.025	36.2	1.7	1.7	0.69
	Reduced XPS[b]	70.0 (2.4)	83.1 (2.3)	0.014	0.025	37.5	1.2	1.8	0.67
	Post CO/O_2	70.6 (3.1)	83.2 (2.4)	0.018	0.022	34.3	2.2	1.2	0.65
Au/SiO_2	Reduced	–	83.5 (2.2)	–	0.028	34.1	6.1	–	0.82

[a] The reduced sample was further reduced in the pretreatment chamber of the XPS facility at 200 °C for 10 min in flowing H_2(10%)/Ar before being re-analyzed.
[b] The reduced sample was further reduced in the pretreatment chamber of the XPS facility at 400 °C for 10 min in flowing H_2(10%)/Ar before being re-analyzed.

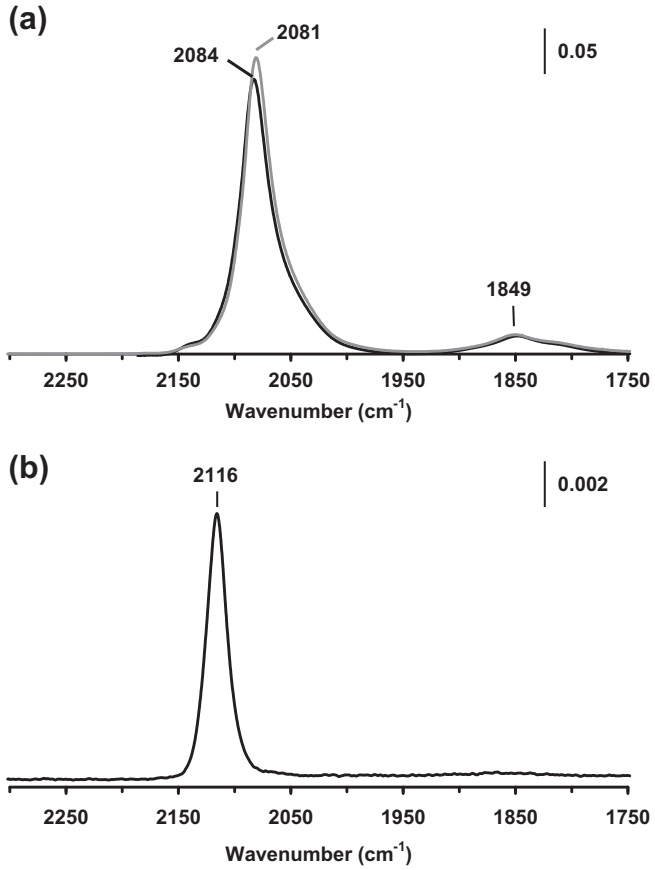

Fig. 7. CO-FTIR spectra of (a) Pt/SiO_2 (— exposed to 1.1 Torr of CO and — after evacuation at RT) and (b) Au/SiO_2 exposed to 1.1 Torr of CO.

can now be seen to consist of a main band at 2046 cm^{-1} and a shoulder at 2064 cm^{-1} (spectrum (i) in Fig. 8b). In contrast, the intensity of the bridged Pt–CO was not significantly affected. The same spectral intensity redistribution from Au–CO to Pt–CO was observed for $AuPt(1.8)/SiO_2$ (not shown). This phenomenon was reversible and reproducible, from a qualitative point of view, upon the re-introduction of CO (Fig. 8).

The broadness of the Pt–CO band in the bimetallic sample in Fig. 8b can be explained by the presence of a variety of different Pt sites available for CO adsorption on the nanoparticle surface. The shift to lower frequency of 39 cm^{-1} of the Pt–CO peak position from the monometallic Pt catalyst (2081 cm^{-1}, Fig. 7a) to that of bimetallic Pt–CO (2042 cm^{-1}) is certainly in part due to a geometric effect resulting from the dilution of Pt sites by Au [49]. This dilution would result in a lower density of adsorbed CO molecules on Pt and therefore a decrease in the dipole–dipole coupling between sites with the same vibration frequency [9,48] (dipole–dipole coupling diminishes at a rate of r^{-3}, where r is the distance between two coupling CO molecules). This indicates that Pt and Au are intimately mixed within and on the surface of individual particles as already proved by Chandler and co-workers [6] and Mihut et al. [12].

More interesting though is the spectral intensity redistribution in the case of bimetallic samples. This has been already observed by Chandler et al. [6] with $AuPt/SiO_2$ samples obtained by deposition of AuPt in dendrimers. They attributed the spectral intensity redistribution, i.e., the increase in intensity of the Pt–CO band as CO molecules are desorbed from the Au sites, to surface restructuring [6,9] and/or screening effect [6] between CO molecules adsorbed onto the two different metals. According to Hollins [48], since the frequency difference between the absorption of Pt–CO (2042 cm^{-1}) and Au–CO (2111 cm^{-1}) is smaller than 100 cm^{-1}, absorption intensity could be redistributed from the lower-frequency peak (Pt–CO) to the higher-frequency peak (Au–CO). This arises from the screening of electric fields from lower-frequency oscillators (Pt–CO), resulting in enhanced absorption by higher-frequency bands (Au–CO). Therefore, as the higher-energy bands are removed, the intensity borrowing from Pt–CO would diminish, increasing the intensity of the Pt–CO band. The screening effect of the Au–CO band on the Pt–CO band could also explain the increase in intensity of the Pt–CO band as CO molecules are desorbed from the Au sites, as observed here (Fig. 8a and b, spectra i).

A shift of 39 cm^{-1} is, however, considerably larger than that expected from coupling effects alone, since it is known that the infrared spectrum of CO adsorbed on platinum typically exhibits a coverage-dependent frequency shift of 30 cm^{-1} [49,50]. Additional experiments (not shown) were performed to determine the Pt–CO singleton frequency ($\nu^{12}CO$ free of dipole–dipole coupling effect) of the Pt/SiO_2 and $AuPt(1.2)/SiO_2$ samples. To achieve this goal, the CO coverage was lowered by evacuation of the samples at increasing temperatures, as reported earlier [50]. The Pt–CO singleton frequency on Pt/SiO_2 was estimated to be 2051 cm^{-1}, in excellent agreement with that reported earlier by Primet via the same methodology and via isotopic dilution of ^{12}CO by ^{13}CO (2052 cm^{-1}) [50], whereas that on $AuPt(1.2)/SiO_2$ was estimated to be 2041 cm^{-1}.

The larger shift was therefore attributed to an electronic effect, a shift in the absorption to lower frequency is indicative of a weakening of the CO bond due to increased back-electron transfer into the CO $2\pi^*$ antibonding orbital. This suggests that the presence of Au has increased the electron density of Pt, as also supported by the XPS data (Section 3.1.6). This electronically induced shift is coherent with previously reported observations on $AuPt/SiO_2$ systems [7,11,12,25]. The possibility of electron transfer from Au to Pt despite the difference in electronegativity has been reported in former studies, as indicated previously in Section 1.

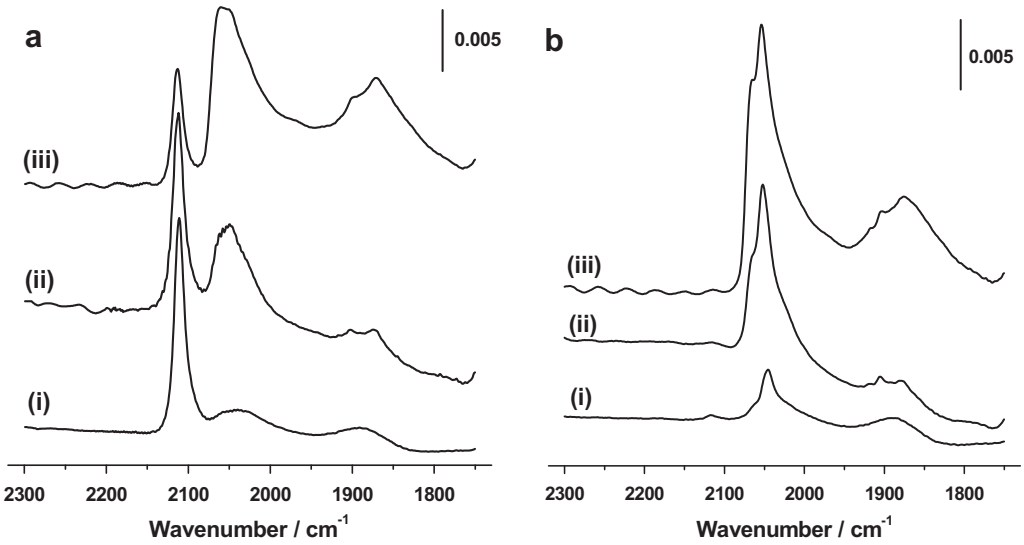

Fig. 8. CO-FTIR spectra of the comparison of consecutive CO exposure-removal cycles on AuPt(1.2)/SiO_2: (a) after CO exposure and (b) after evacuation (10^{-6} mbar, RT, 0.5 h), (i) 1st cycle (1.1 Torr CO, RT, 0.1 h), (ii) 2nd cycle (4 Torr CO, RT, 18 h), (iii) 3rd cycle (10.5 Torr CO, 100 °C, 18 h).

The change in the absorbance bands of AuPt(1.2)/SiO_2 was investigated further (Fig. 8). Two further cycles of CO exposure-evacuation were performed on AuPt(1.2)/SiO_2 (spectra ii and iii in Fig. 8). After the first cycle of CO adsorption–desorption (spectra i), the catalyst was again exposed to CO, this time at higher CO pressure and for a longer duration (4 Torr, 18 h, RT). After confirmation that CO was re-adsorbed onto Au atoms (Fig. 8a, spectrum (ii)), the CO was evacuated (10^{-6} mbar, RT) and the spectrum recorded again (Fig. 8b, spectrum (ii)) showing as before the increased and narrowed Pt–CO band. The catalyst was again, exposed to CO, a third time, at even higher CO pressure at 100 °C (10.5 Torr CO, 18 h, 100 °C) (spectra iii). It is clear regarding these three CO adsorption–desorption spectra (Fig. 8), that the intensity of the Au–CO band diminishes and that of the two Pt–CO bands increases with each cycle and prolonged exposure to CO. The increase in intensity of the Pt–CO bands observed after further exposure to CO at elevated temperatures in combination with the decrease in the Au–CO peak intensity is good argument/evidence for a restructuring of the nanoparticles, as Pt migrates outwards, replacing Au at the nanoparticle surface. The restructuring can be explained thermodynamically since CO chemisorbs to Pt more strongly than to Au and provides a driving force for pulling Pt to the particle surface [19]. The surface energy of the nanoparticle will be reduced by the increased bond formation with CO if Pt is at the surface.

3.1.8. Summary on the characterization of the bimetallic nanoparticles

All these results provide evidence for the formation of bimetallic AuPt particles the structure of which evolves with environment. When the AuPt particles are still in solution and polymer stabilized, the structure is Au_{core}–Pt_{shell} according to former interpretation of the UV–Vis spectra [14]. After deposition onto silica and drying, they become alloy-type with surface enrichment by Au according to the XPS data, despite bulk AuPt having a large miscibility gap extending from 18% to 98 % Pt [19], these results show consistently, as with former studies on supported AuPt catalysts arising from organobimetallic precursors [11,12], preformed particles in dendrimers [9], vapor deposition [26] and in colloidals [36], that bimetallic AuPt particles can be obtained. Moreover, as also reported in [9,26,37], the bimetallic nanoparticles consist of an alloy-type structure. Under pure CO, further Pt enrichment occurs, but Au is still present on the surface, as also shown by Chandler and co-workers [6,9].

3.2. Catalytic results

3.2.1. Benzene hydrogenation

Benzene hydrogenation experiments were performed on all catalysts at either 50 °C and/or 115 °C. Pt-based catalysts are known to efficiently catalyze this reaction, and for this reason, it can be considered as a test-reaction. Reaction rates are summarized in Table 3. As expected, the monometallic Pt/SiO_2 catalyst was active at the lower temperature, and monometallic Au/SiO_2 was inactive at both temperatures. AuPt(1.8)/SiO_2 was also found to be inactive at both temperatures. AuPt(1.2)/SiO_2 was inactive at 50 °C, but active at 115 °C. In order to compare the hydrogenation rate of Pt/SiO_2 and AuPt(1.2)/SiO_2, it is first necessary to extrapolate the rate of the Pt/SiO_2 to 115 °C. This can be achieved since it is known that the rate of reaction of benzene hydrogenation can be represented by [59]:

$$Rate = k[benzene]^0[H_2]^0, \quad \text{where } k = e^{-E_a/RT} \tag{1}$$

thus allowing extrapolation of the hydrogenation rate to 115 °C, as shown in the following equation:

$$\frac{Rate_{T_1}}{Rate_{T_2}} = \frac{k_{T_1}}{k_{T_2}} \tag{2}$$

The activation energy of benzene hydrogenation over a Pt/SiO_2 catalyst is known to be 47.4 kJ mol^{-1} [59]. Reaction rates are converted into turnover rates (TOR), the rate of reaction per Pt surface atom, taking into account the Pt dispersion. The number of Pt surface atoms was calculated using the chemisorption data for Pt/SiO_2 (Section 3.1.4) and the average particle diameters determined by TEM for AuPt/SiO_2 (Section 3.1.5) and the method previously described in [35]. In the bimetallic case, TOR is calculated assuming the nanoparticles are homogeneous alloys in the bulk and on the surface.

Table 3
Rate of reaction of benzene hydrogenation over each catalyst at two reaction temperatures (n.d. = not determined, * = calculated).

Catalyst	Rate ($\times 10^{-8}$ mol s^{-1} g^{-1})		TOR (s^{-1})	
	50 °C	115 °C	50 °C	115 °C
Pt/SiO_2	530	n.d.	0.17	3.20*
AuPt(1.2)/SiO_2	0	14	0	0.03*
AuPt(1.8)/SiO_2	0	0	0	0
Au/SiO_2	0	0	0	0

The benzene hydrogenation turnover rate of Pt/SiO_2 at 50 °C is 0.17 s^{-1}, which is comparable with data reported previously [59] and extrapolates to 3.20 s^{-1} at 115 °C (Table 3). The TOR for the Pt surface atoms of the bimetallic $AuPt(1.2)/SiO_2$ catalyst at 115 °C is found to be 0.03 s^{-1}, which is considerably lower than that of Pt/SiO_2 (3.20 s^{-1}) (Table 3). The activity of the bimetallic catalyst toward benzene hydrogenation is therefore considerably lower than expected when the particles are assumed to be homogeneous alloys. These results suggest that the presence of gold inhibits the reactivity of Pt in benzene hydrogenation; this can be due to an electronic effect resulting from gold proximity that modifies the electronic properties of Pt as attested by the XPS and FTIR results (Section 3.1.6 and 3.1.7).

The fact that $AuPt(1.8)/SiO_2$ is as inactive as the monometallic Au catalyst is consistent with the lower proportion of Pt than in $AuPt(1.2)/SiO_2$.

Benzene hydrogenation of unsupported AuPt alloys of different compositions has been investigated previously [60]. It has been suggested that successful benzene hydrogenation requires ensembles of Pt atoms, if Pt sites became too diluted by Au, activity is no longer observed, which is coherent with the observations reported here.

3.2.2. CO oxidation

Given the much greater Pt content of Pt/SiO_2 compared with the $AuPt/SiO_2$ samples (Table 2), Fig. 9 shows that Pt/SiO_2 is very active in the reaction of CO oxidation at 280 °C, whereas Au/SiO_2 is poorly active (it is well known that gold nanoparticles supported on silica hardly catalyze CO oxidation [61,62]). The bimetallic catalysts exhibit an intermediate activity, and $AuPt(1.2)/SiO_2$ is about three times more active than $AuPt(1.8)/SiO_2$, even though the content of Pt in $AuPt(1.2)/SiO_2$ is only 40% greater than in $AuPt(1.8)/SiO_2$ (Table 1).

The activation energies of CO oxidation by O_2 over each catalyst are shown in Table 4. Interestingly, it can be seen that the activation energy of $AuPt(1.2)/SiO_2$ is comparable to that of Pt/SiO_2 and in good agreement with those reported on supported Pt catalysts [63,64] in a temperature domain close to that studied in the present work, whereas that of $AuPt(1.8)/SiO_2$ is comparable to that of Au/SiO_2. The activation energy found on Au/SiO_2 in this study is slightly lower than that reported by Chandler and co-workers [6]. In contrast, these authors reported a much lower activation energy on Pt/SiO_2 than that found in the present work. It should be noted, however, that Chandler and co-workers determined this activation energy at much lower temperatures than in the present study and that Cant et al. [28] showed that the activation energy of the CO oxidation reaction on Pt/SiO_2 had a tendency to decrease with decreasing reaction temperatures.

The plots used for the determination of the reaction orders summarized in Table 4 are shown in Fig. 9. The reaction orders for Pt/SiO_2 were −0.88 with respect to CO and 1.02 with respect to O_2, which is in good agreement with those reported previously in the same temperature range [63,64]. For Au/SiO_2, the reaction orders were 0.09 with respect to CO and 0.69 with respect to O_2. What is immediately clear from these results is that the reaction rate is dependent on the concentration of CO when the reaction CO/O_2 is catalyzed by Pt/SiO_2, but is near-independent of the CO concentration when catalyzed by Au/SiO_2. The negative reaction order with respect to CO found on Pt/SiO_2 is a result of the very strong bonding of CO with Pt, which inhibits CO oxidation [63–65]. The Au–CO bond is much weaker than the Pt–CO bond, as already attested by the CO-FTIR results (Figs. 7 and 8), which results in the lack of any inhibiting effect on the reaction rate of CO oxidation for Au catalysts. However, in the present case, the reactivity of Au/SiO_2 is very low; this is because gold is poorly efficient at activating oxygen [30] and that when supported on a reducible support, such as titania, the addition of water is usually necessary to activate oxygen [66].

From the CO and O_2 reaction orders measured on $AuPt(1.8)/SiO_2$ (Table 4), which exhibits the lower proportion of Pt, it can be concluded that CO oxidation proceeds exclusively on the Au surface atoms, which is also fully coherent if one compares the reactions orders to those of Au/SiO_2 and with the lack of activity in benzene hydrogenation of this particular sample (Table 3). The bimetallic catalyst with a priori more Pt at the surface ($AuPt(1.2)/SiO_2$) behaves in a manner which is between that of the monometallic Au and Pt catalysts (Table 4), with CO oxidation occurring predominantly on the Pt surface atoms. The less negative order with respect to CO for $AuPt(1.2)/SiO_2$ compared to Pt/SiO_2 can be explained as a reduction in the inhibiting nature of Pt–CO when Au is present.

CO oxidation turnover rates were 6×10^{-4} s^{-1} for Au/SiO_2 and 0.57 s^{-1} for Pt/SiO_2 (Table 5). The value for Pt/SiO_2 is in good agreement with that obtained by Cant et al. [28] (0.4–0.7 s^{-1}, extrapolated from the given data to obtain the appropriate value at 280 °C using the same methodology as that described for benzene hydrogenation turnover rates (please refer to Eq. (2))).

Given the difference in the composition of the bimetallic nanoparticles and the difference in metal loadings and dispersions in each catalyst (Tables 1 and 5), comparison of the CO_2 production rates of the bimetallic catalysts with that determined experimentally on Pt/SiO_2 can be achieved by calculating their expected CO_2 turnover rates by making assumptions about the Pt surface composition of the bimetallic nanoparticles, as the CO_2 turnover rate on Au sites (6×10^{-4} s^{-1}) has been shown to be negligible with respect to that of Pt (0.57 s^{-1}).

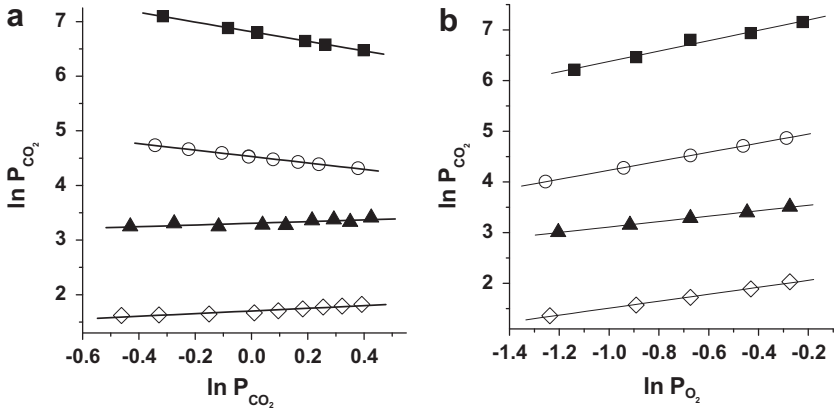

Fig. 9. Kinetic Studies at 280 °C of supported nanoparticle catalysts (■ Pt/SiO_2, ○ $AuPt(1.2)/SiO_2$, ▲ $AuPt(1.8)/SiO_2$, ◇ Au/SiO_2).

Table 4
Kinetic parameters (activation energies and reaction orders) of the CO oxidation reaction at a temperature of 280 °C.

Catalyst	E_a (kJ mol^{-1})	Reaction order		Least square fit, R^2	
		CO	O_2	CO	O_2
Pt/SiO_2	112	−0.88	1.02	0.999	0.982
$AuPt(1.2)/SiO_2$	102	−0.62	0.89	0.996	1.000
$AuPt(1.8)/SiO_2$	55	0.10	0.54	0.540	0.999
Au/SiO_2	64	0.09	0.69	0.985	0.996

Table 5 lists the CO_2 turnover rates calculated for the bimetallic samples assuming that the SiO_2-supported nanoparticles are homogeneous in terms of size and shape, and that the surface composition of the bimetallic nanoparticles can be deduced from (i) the metal dispersion and chemical analysis (making, here, the assumption that the nanoparticles are homogeneous alloys in the bulk and on the surface, Table 1) and (ii) the rate of benzene hydrogenation and the corresponding turnover rates on Pt and Au (Table 3). Differences between the calculated and measured rates can be interpreted as either promotional or inhibiting effects due to the presence of a second metal.

For $AuPt(1.2)/SiO_2$, the calculated CO_2 turnover rates are greater than that determined experimentally on Pt/SiO_2 (0.57 s^{-1}, Table 5). The greatest turnover rate was that calculated using the results of the benzene hydrogenation. Even the CO_2 turnover rate calculated for a homogeneous alloy (1.50 s^{-1}), which overestimates the amount of Pt at the catalyst surface according to the chemisorption and CO-FTIR data, is greater than the turnover rate on Pt/SiO_2 (0.57 s^{-1}).

In the presence of CO at the reaction temperature of 280 °C, one may argue however, that the bimetallic nanoparticles of $AuPt(1.2)/SiO_2$ have rearranged and exposed a number of Pt surface sites greater than that corresponding to the composition of the homogeneous alloy. Even if one considers the extreme situation for which all of the bimetallic particles of $AuPt(1.2)/SiO_2$ have rearranged in such a way that they exposed only Pt atoms at their surface, which is known however to be unlikely from a thermodynamic point of view and the XPS and FTIR results, the corresponding CO_2 turnover rates would be estimated to be 0.67 s^{-1}, which is still greater than the turnover rate determined on Pt/SiO_2 (0.57 s^{-1}). This is evidence that $AuPt(1.2)/SiO_2$ is experiencing a promotional effect due to the combination of Au and Pt, and this confirms the synergistic effect between Au and Pt announced in the introduction.

To account for the observed changes in the CO and O_2 orders and the synergistic effect between the two metals for the CO oxidation reaction in $AuPt(1.2)/SiO_2$, it is proposed that an electronic effect in the AuPt bimetallic nanoparticles with an electron transfer from Au to Pt lowers the Pt–CO bond energy in agreement with the CO-FTIR results of the present study, which favors O_2 activation on platinum.

In the case of PtAu alloys, it has been reported that CO would be more strongly bound to Pt in PtAu alloys than on a pure Pt sample [9,67,68]. Such a conclusion, with a promotional effect of Au on the CO oxidation reaction in $AuPt(1.2)/SiO_2$, is however, rather controversial as CO should be less reactive if more strongly chemisorbed to Pt. It must be stressed, nonetheless, that Pedersen et al. also reported the existence of Pt sites in diluted PtAu alloys for which CO is less strongly bound than in pure Pt [68]. These particular Pt sites could be responsible for the synergistic effect observed in AuPt alloys. The fact that CO would be less strongly bound to these Pt sites would be coherent with an increased electron density of these Pt surface atoms due to charge transfer from Au to Pt, as indicated by the CO-FTIR results. This increased electron density would result in a decrease of the strength of the Pt–CO bond, as CO is known to be a weak base [69], and therefore in a decreased CO coverage favoring O_2 dissociative adsorption followed by reaction with CO adsorbed on Pt and may be also on Au, i.e., favoring the CO oxidation kinetics. This increased electron density of the Pt sites and the particle surface enriched by gold would also account for the decreased activity of the AuPt alloys for benzene hydrogenation, in agreement with previously reported studies on the hydrogenation of aromatics on electron-enriched Pt sites [70,71].

The results for $AuPt(1.8)/SiO_2$ are however not consistent with this interpretation. For this catalyst, the kinetic orders are close to those of Au/SiO_2 and the calculated CO_2 turnover rate based on a surface composition of the homogeneous alloy is much lower (0.01 s^{-1}) than the measured turnover rate on Pt/SiO_2 (0.57 s^{-1}, Table 5). This suggests that there may be a 'compositional limit' for the promotional effect of Au toward Pt and that there is a point at which Pt surface atom dilution becomes too great for this to occur. This could be confirmed by looking at other AuPt compositions.

4. Conclusion

Bimetallic core–shell AuPt nanoparticles have been prepared by radiolysis and deposited onto silica. After stabilizer decomposition, the resulting catalysts have been shown to contain alloy AuPt nanoparticles with a surface enriched by gold according to XPS, indicating particle restructuring. The Pt–CO band observed in FTIR-CO spectroscopy was found to be screened by the Au–CO band confirming the close proximity of the two metals at the nanoparticle surface. FTIR-CO spectroscopy gave evidence for further restructuring of the AuPt particles with the migration of Pt toward the surface in the presence of CO. However, Au seems to remain predominant on the surface according to XPS and catalytic results.

Gold in the bimetallic particles has been shown to inhibit the catalysis of benzene hydrogenation and to promote the catalysis of CO oxidation by O_2 at least for the $AuPt(1.2)/SiO_2$ sample.

Table 5
CO oxidation reaction rates for each catalyst at 280 °C under stoichiometric conditions (1% CO–0.5% O_2 in He).

Catalyst	D (%)[a]	Measured CO_2 rate[d]	TOR (s^{-1})[e]		
			Experimental	Calculated	
				Homogeneous alloy	Benzene hydrogenation
Pt/SiO_2	31.7[b]	18,000	0.57		
$AuPt(1.2)/SiO_2$	24.9[c]	6900		1.50	162
$AuPt(1.8)/SiO_2$	25.0[c]	34		0.01	
Au/SiO_2	31.4[c]	7	0.0006		

[a] Metal dispersion.
[b] From H_2 and CO chemisorption data (Section 3.1.4).
[c] From TEM (Section 3.1.5).
[d] $\times 10^{-9}$ mol CO_2 s^{-1} g^{-1}.
[e] Rate of reaction per Pt surface atom.

AuPt(1.8)/SiO_2 was found to inhibit both reactions, suggesting that there is a compositional limit to the promotional effect which can occur in bimetallic AuPt/SiO_2 toward CO oxidation. The observed synergistic effect between the two metals and the changes in the CO and O_2 orders of AuPt(1.2)/SiO_2 compared to Pt/SiO_2 are attributed to an electronic effect in the AuPt bimetallic nanoparticles with an electron transfer from Au to Pt, as indicated by XPS and CO-FTIR.

Acknowledgments

This work was supported by the Region Ile-de-France in the framework of C'Nano IdF. C'Nano IdF is the centre of competences in nanosciences for the Paris region, supported by CNRS, CEA, MESR and the region Ile-de-France. The authors also thank Dr. J. Blanchard and Dr. L. Delannoy for fruitful discussions about chemisorption on Pt, and CO-FTIR on Au and alloy restructuring, respectively.

References

[1] J.M. Thomas, R. Raja, B.F.G. Johnson, S. Hermans, M.D. Jones, T. Khimyak, Ind. Eng. Chem. Res. 42 (2003) 1563.
[2] L.M. Bronstein, D.M. Chernyshov, I.O. Volkov, M.G. Ezernitskaya, P.M. Valetsky, V.G. Matveeva, E.M. Sulman, J. Catal. 196 (2000) 302.
[3] N. Toshima, M. Harada, Y. Yamazaki, K. Asakura, J. Phys. Chem. 96 (1992) 9927.
[4] M. Harada, K. Asakura, Y. Ueki, N. Toshima, J. Phys. Chem. 96 (1992) 9730.
[5] O.S. Alexeev, B.C. Gates, Ind. Eng. Chem. Res. 42 (2002) 1571.
[6] B.J. Auten, H.F. Lang, B.D. Chandler, Appl. Catal. B: Environ. 81 (2008) 225.
[7] J.H. Zeng, J. Yang, J.Y. Lee, W.J. Zhou, J. Phys. Chem. B 110 (2006) 24606.
[8] A. Habrioux, E. Sibert, K. Servat, W. Vogel, K.B. Kokoh, N. Alonso-Vante, J. Phys. Chem. B 111 (2007) 10329.
[9] H.G. Lang, S. Maldonado, K.J. Stevenson, B.D. Chandler, J. Am. Chem. Soc. 126 (2004) 12949.
[10] X.H. Peng, Q.M. Pan, G.L. Rempel, Chem. Soc. Rev. 37 (2008) 1619.
[11] E. Bus, J.A. van Bokhoven, J. Phys. Chem. C 111 (2007) 9761.
[12] C. Mihut, C. Descorme, D. Duprez, M.D. Amiridis, J. Catal. 212 (2002) 125.
[13] H. Remita, I. Lampre, M. Mostafavi, E. Balanzat, S. Bouffard, Radiat. Phys. Chem. 72 (2005) 575.
[14] F. Ksar, L. Ramos, B. Keita, L. Nadjo, P. Beaunier, H. Remita, Chem. Mater. 21 (2009) 3677.
[15] J. Belloni, H. Remita, in: M. Spotheim-Maurizot, M. Mostafavi, T. Douki, J. Belloni, Radiation Chemistry: From Basics to Applications in Material and Life Sciences, EDP Sciences, 2008, p. 97.
[16] J. Belloni, M. Mostafavi, H. Remita, J.L. Marignier, M.O. Delcourt, New J. Chem. 22 (1998) 1239.
[17] J. Belloni, Catal. Today 113 (2006) 141.
[18] W. Abidi, H. Remita, Recent Patents Eng. 4 (2010) 170.
[19] R. Bouwman, W.M. Sachtler, J. Catal. 19 (1970) 127.
[20] A.Y. Stakheev, L.M. Kustov, Appl. Catal. A 5 (1983) 85.
[21] S.J. Tauster, Acc. Chem. Res. 20 (1987) 389.
[22] J.D. Bracey, R. Burch, J. Catal. 86 (1984) 384.
[23] P. Hernandez-Fernandez, S. Rojas, P. Ocon, J.L.G. de la Fuente, J.S. Fabian, J. Sanza, M.A. Pena, F.J. Garcia-Garcia, P. Terreros, J.L.G. Fierro, J. Phys. Chem. C 111 (2007) 2913.
[24] A. Sachdev, J. Schwank, J. Catal. 120 (1989) 353.
[25] H. Tada, F. Suzuki, S. Ito, T. Akita, K. Tanaka, T. Kawahara, H. Kobayashi, J. Phys. Chem. B 106 (2002) 8714.
[26] M.F. Luo, C.C. Wang, G.R. Hu, W.R. Lin, C.Y. Ho, Y.C. Lin, Y.J. Hsu, J. Phys. Chem. C 113 (2009) 21054.
[27] R.E. Watson, J.W. Davenport, M. Weinert, Phys. Rev. B 35 (1987) 508.
[28] N.W. Cant, P.C. Hicks, B.S. Lennon, J. Catal. 54 (1978) 372.
[29] V. Aguilar-Guerrero, B.C. Gates, Catal. Lett. 130 (2009) 108.
[30] B.D. Chandler, C.G. Long, J.D. Gilbertson, C.J. Pursell, G. Vijayaraghavan, K.J. Stevenson, J. Phys. Chem. C 114 (2010) 11498.
[31] L. Delannoy, N. El Hassan, A. Musi, N.N. Le To, J.M. Krafft, C. Louis, J. Phys. Chem. B 110 (2006) 22471.
[32] M.C. Daniel, D. Astruc, Chem. Rev. 104 (2004) 293.
[33] S. Link, M.A. El-Sayed, J. Phys. Chem. B 103 (1999) 8410.
[34] M. Mirdamadi-Esfahani, M. Mostafavi, B. Keita, L. Nadjo, P. Kooyman, H. Remita, Gold Bull. 43 (2010) 49.
[35] G. Bergeret, P. Gallezot, in: G. Ertl, H. Knozinger, J. Weitkamp (Eds.), Handbook of Heterogeneous Catalysis, vol. 2, Wiley-VCH, 1997, p. 439.
[36] J. Luo, M.M. Maye, V. Petkov, N.N. Kariuki, L.Y. Wang, P. Njoki, D. Mott, Y. Lin, C.J. Zhong, Chem. Mater. 17 (2005) 3086.
[37] G.C. Bond, Platinum Met. Rev. 51 (2007) 63.
[38] C.X. Xu, R.Y. Wang, M.W. Chen, Y. Zhang, Y. Ding, Phys. Chem. Chem. Phys. 12 (2010) 239.
[39] E. Irissou, F. Laplante, S. Garbarino, M. Chaker, D. Guay, J. Phys. Chem. C 114 (2010) 2192.
[40] Y. Xu, Y. Dong, J. Shi, M. Xu, Z. Zhang, X. Yang, Catal. Commun. 13 (2011) 54.
[41] J. Radnik, C. Mohr, P. Claus, Phys. Chem. Chem. Phys. 5 (2003) 172.
[42] V. Pitchon, A. Fritz, J. Catal. 186 (1999) 64.
[43] H.B. Liu, U. Pal, J.A. Ascencio, J. Phys. Chem. C 112 (2008) 19173.
[44] A. Hugon, L. Delannoy, J.M. Krafft, C. Louis, J. Phys. Chem. C 114 (2010) 10823.
[45] F. Gao, Y.L. Wang, D.W. Goodman, J. Phys. Chem. C 113 (2009) 14993.
[46] F. Gao, Y.L. Wang, D.W. Goodman, J. Am. Chem. Soc. 131 (2009) 5734.
[47] S.M. Oxford, P.L. Lee, P.J. Chupas, K.W. Chapman, M.C. Kung, H.H. Kung, J. Phys. Chem. C 114 (2010) 17085.
[48] P. Hollins, Surf. Sci. Rep. 16 (1992) 51.
[49] P.T. Fanson, W.N. Delgass, J. Lauterbach, J. Catal. 204 (2001) 35.
[50] M. Primet, J. Catal. 88 (1984) 273.
[51] M.A. Bollinger, M.A. Vannice, Appl. Catal. B: Environ. 8 (1996) 417.
[52] J.D. Grunwaldt, M. Maciejewski, O.S. Becker, P. Fabrizioli, A. Baiker, J. Catal. 186 (1999) 458.
[53] S. Minico, S. Scire, C. Crisafulli, A.M. Visco, S. Galvagno, Catal. Lett. 47 (1997) 273.
[54] D.J.C. Yates, J. Colloid Interface Sci. 224 (1969) 36.
[55] R. Meyer, C. Lemire, Sh.K. Shaikhutdinov, H.-J. Freund, Gold Bull. 37 (2004) 72.
[56] H.K.M. Mihaylov, K. Hadjiivanov, B.C. Gates, Chemie Ingenieur Technik 79 (2007) 795.
[57] F. Boccuzzi, A. Chiorino, M. Manzoli, D. Andreeva, T. Tabakova, J. Catal. 188 (1999) 176.
[58] J.Y. Lee, J. Schwank, J. Catal. 102 (1986) 207.
[59] L. Salin, C. Potvin, J.F. Tempere, M. Boudart, G. Djega-Mariadassou, J.M. Bart, Ind. Eng. Chem. Res. 37 (1998) 4531.
[60] S. Puddu, V. Ponec, Rec. Trav. Chim. 95 (1976) 255.
[61] M. Haruta, S. Tsubota, T. Kobayashi, H. Kageyama, M.J. Genet, B. Delmon, J. Catal. 144 (1993) 175.
[62] M. Haruta, H. Kageyama, N. Kamijo, T. Kobayashi, F. Delannay, T. Inui, Stud. Surf. Sci. Catal., Elsevier (33).
[63] Y.F. Yu Yao, J. Catal. 87 (1984) 152.
[64] R.H. Nibbelke, M.A.J. Campman, J.H.B.J. Hoebink, G.B. Marin, J. Catal. 171 (1997) 358.
[65] I. Manuel, K. Chaubet, C. Thomas, H. Colas, N. Matthess, G. Djega-Mariadassou, J. Catal. 224 (2004) 269.
[66] G.C. Bond, C. Louis, D. Thompson, Catalysis by Gold, Imperial College Press, 2006.
[67] X.B. Ge, X.L. Yan, R.Y. Wang, F. Tian, Y. Ding, J. Phys. Chem. C 113 (2009) 7379.
[68] M.O. Pedersen, S. Helveg, A. Ruban, I. Stensgaard, E. Laegsgaard, J.K. Norskov, F. Besenbacher, Surf. Sci. 426 (1999) 395.
[69] K.I. Hadjiivanov, G.N. Vayssilov, Adv. Catal. 47 (2002) 307.
[70] A. de Mallmann, D. Barthomeuf, J. Chim. Phys. 87 (1990) 535.
[71] D.E. Ramaker, J. de Graaf, J.A.R. van Veen, D.C. Koningsberger, J. Catal. 203 (2001) 7.